HADRONIC MATTER PROPERTIES FROM THE REACTION STUDIES AT SIS*

N. Herrmann[a] and K. Wiśniewski[a,b]

For the FOPI Collaboration

[a]Physikalisches Institut, Universität Heidelberg
Philisophenweg 12, 69120 Heidelberg, Germany
[b]Institute of Experimental Physics, Warsaw University
Hoża 69, 00-681 Warszawa, Poland

(Received February 11, 2004)

We present recent results of heavy-ion experiments performed by the FOPI collaboration at the SIS accelerator in Darmstadt. The studied observables, such as the isotopic ratios, the flow of nuclear fragments and their rapidity density distributions, provide necessary information to judge about the dynamics of heavy-ion reactions at intermediate energies. Comparison of the measured yields of strange- and anti-strange particles allows to conclude about the production of normally not measured Σ^+ and Σ^- hyperons.

PACS numbers: 25.75.Ld, 25.70.Pq, 25.75.Dw

1. Introduction

Heavy-ion experiments at intermediate beam energies (of up to a few GeV per nucleon) are often considered to be a "laboratory" to investigate the properties of the dense and/or highly excited nuclear matter. The aim is to probe the nuclear equation of state (EOS) far from the saturation point [1] and, more recently, to learn about the in-medium modifications of hadron properties in the nuclear environment [2]. This knowledge is relevant not only for the hadron and nuclear physics. It has also a great impact on the astrophysics and cosmology. Dense hadronic matter is found, for example, in the interior of neutron stars. A highly exited and hot state is believed to exist shortly after the Big Bang.

* Presented at the XXVIII Mazurian Lakes School of Physics, Krzyże, Poland, August 31–September 7, 2003.

There are obvious differences between a finite nuclear system formed for a few tens of fm/c in the laboratory and the matter existing on large scales. Surface and non-equilibrium effects, which are small in the case of the bulk matter, play an important role in heavy-ion experiments. Microscopic BUU- or QMD-type calculations, used to model reactions of heavy ions, are believed to provide a necessary link between experimental data and the properties of matter that are studied. Important dynamical aspects like, for instance, the momentum dependence of the mean fields can be taken into account in such calculations. Non-equilibrium effects caused by the separation of the projectile- and the target-nucleons in the phase space can be also accounted for [3].

In fact only the lack of equilibration gives a hope that the memory of the conditions in which properties of the system should be probed is preserved, at least partially, till the end of a reaction. Otherwise, observables measured in the final state could reflect only freeze-out conditions of a dilute system as anticipated by theories based on thermal models [4]. One of the observables which develops in the course of a reaction and which is thought to provide information about the early phase of a collision is the flow of nuclear fragments. Originating from pressure gradients and being dynamical, non-equilibrium effects, many types of flow are expected to depend strongly on the stiffness of the EOS [5]. Yields and phase-space distributions of produced strange particles are, in addition, believed to reveal the in-medium modifications of hadrons [6].

In this contribution we present recent results obtained by the FOPI collaboration, which hopefully will help to understand better the dynamics of heavy-ion collisions at intermediate energies and the properties of the hadronic matter at high densities. The paper is organized as follows. In Section 2 we recall very briefly the most relevant features of the FOPI apparatus. In Section 3 we concentrate on the question of equilibration. We report on the results from the experiment in which the phase-space distributions of the reaction products were measured for different target-projectile combinations of isobars with the mass number $A = 96$. The analysis of the yields-ratios addresses in a model-independent way the question of transparency and mixing of the participant matter. Furthermore, we present the systematic studies on transverse-rapidity distributions and directed sideflow of protons in systems of different sizes and beam energies. With this the question of stopping in nuclear collisions is addressed. In Section 4 we turn to the produced strange particles. We present the measured K^0meson and Λ hyperon phase-space distributions for the Ni+Ni system at 1.93 AGeV beam energy, and try to extract the usually not measured Σ hyperon yields. We also mention preliminary results on an interesting study of Λ-deuteron correlations, which may provide evidence for the formation of ultra-dense clusters and for the in-medium modifications of anti-kaons. Section 5 contains the conclusions and outlook.

2. FOPI detector

The FOPI detector is a large acceptance, modular system for fixed target experiments. It is located at the beam line of the heavy-ion accelerator SIS in Darmstadt. The results reported in this contribution were obtained partially from the newest, high-statistics experiments performed after the last upgrade of the detector (K^0, Λ, Λ-d correlations), and partially are based on some older data, which were systematically collected during many years of running, and of which compilation was completed only in the newer experiments (isotopic ratios, stopping, sideflow). Systems from light, Ca–Ca, to heavy, Au–Au, were investigated at incident beam kinetic energies between 150 and 1930 MeV per nucleon. In this place it is impossible to review the details of all the experiments referred to hereafter. Therefore, here we recall only the most important facts and refer the reader to the details about the FOPI detector reported in the literature [7].

The FOPI detector is axially symmetric around the beam axis, and has almost complete azimuthal angle coverage. The essential part of the setup consist of the two drift chambers: the CDC and the Helitron. Charged-particle trajectories are tracked in the magnetic field, which loses its homogeneity at distances larger than 1.2 meters from the target in the beam direction. The geometric acceptance of the CDC corresponds to the target-rapidity region, whereas the Helitron covers the area around the mid-rapidity. Not only the momenta of particles are determined, but also their specific energy loss is measured in both drift chambers. Particle identification is completed by the TOF measurements, performed with the two sets of scintillator arrays: the Plastic Wall, in the forward region, and the Barrel, in the backward center-of-mass hemisphere. In this way, in most of the cases a redundancy is achieved in particle mass determination. In addition, isotops can be separated with respect to their charges.

Due to the large geometric acceptance, the centrality and the reaction plane of collisions can be determined with a good accuracy on an event-by-event basis. Usually the correlation between the multiplicity of the reaction products and the centrality of a collision is exploited. The estimate of the impact parameter of a given reaction is based on the measured differential cross-section for the multiplicity distribution and the geometrical sharp-cut approximation. The estimate can be also based on the ratio of the transverse to the longitudinal kinetic energies of detected fragments, E_{rat}. Due to the fluctuations of the measured multiplicities, the second method gives a better sensitivity to small changes of the impact parameter for more central reactions. The reaction plane of a collision is determined in a standard way by summing up the transverse components of the momenta of the detected fragments.

Figure 1 shows a typical momentum-space distribution of particles detected in central ($b < 2$ fm) Ru+Ru collisions at 400 AMeV beam kinetic energy. At this bombarding energy, nucleons and fragments are the majority of the reaction products. In figure 1 only $Z = 1$ fragments are included. A representation in terms of the transverse momentum and the rapidity is chosen. The momenta are normalized to masses of fragments, and the rapidities are scaled to the beam rapidity. In this representation $-1, 0$ and 1 correspond to the target-, mid- and projectile-rapidities, respectively. A small gap in the acceptance between the forward part (Helitron and Plastic Wall) and the backward part (CDC and Barrel) of the detector can be seen in figure 1. Nevertheless, one can notice that the momentum-space distribution is peaked at mid-rapidity, which suggests that the participant matter is stopped to a large extent.

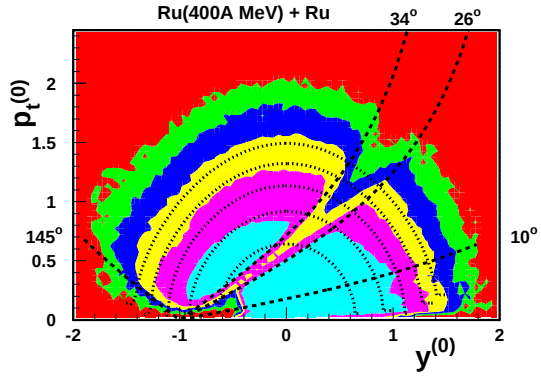

Fig. 1. Phase-space distribution of the $Z = 1$ reaction products in central ($b < 2$ fm) Ru+Ru collisions at 400 AMeV beam kinetic energy.

3. Stopping and mixing

The question of stopping was addressed in more detail in an experiment in which $^{96}_{44}$Ru and $^{96}_{40}$Zr nuclei were used in four different target-projectile combinations [8]. The isospin (N/Z) ratios of the Ru and Zr isobars of the same mass number, $A = 96$, are different and equal to 1.18 and 1.40, respectively. Therefore, one expects, a little more protons to be detected in the Ru+Ru than in the Zr+Zr reactions at the same beam energy. For the mixed systems (Ru+Zr and Zr+Ru), the number of produced protons ought to be between the two values of the symmetric reactions. The results for different target-projectile combinations can be easier compared if the ratio:

$$R_Z = \frac{2Z - Z^{\mathrm{Ru}} - Z^{\mathrm{Zr}}}{Z^{\mathrm{Zr}} - Z^{\mathrm{Ru}}} \tag{1}$$

is studied. Z^{Ru}, Z^{Zr} and Z correspond to the number of protons detected in the Ru+Ru, Zr+Zr, and in the considered reaction, respectively. By definition, R_Z equals to -1 for the Ru+Ru and to $+1$ for the Zr+Zr system. For other systems, the values of R_Z can be calculated in different regions of the phase space.

Plots in the upper part of figure 2 show the rapidity dependence of the R_Z ratio obtained for central ($b < 2$ fm) Ru+Zr and Zr+Ru collisions at two bombarding energies: 400 and 1500 AMeV. The results for the higher energy are still preliminary. The ratios were extracted in the backward hemisphere. In each case the number of protons, Z, was taken as the number of the identified protons plus the number of protons bound in the detected deuterons. Because of the symmetry, the results for both systems show the same, though opposite in sign, trend. At mid-rapidity, the values of R_Z approach zero by necessity. However, both the positive values of R_Z found for the Ru+Zr system in the backward hemisphere as well as the negative values extracted in the case of the Zr+Ru system for the negative scaled rapidities allow to conclude that this region of the phase-space is populated mostly by the target-nucleons. This observation is compatible with an assumption that at both considered energies the target- and the projectile-nucleons did not get fully mixed in the course of the reactions.

Obviously R_Z seems to depend linearly on the isospin ratio of the system. The total measured rapidity density distribution, $\frac{dN}{dy^{(0)}}$, can be deconvoluted into separate distributions for the target- and the projectile-nucleons:

$$\frac{dN^{\frac{\mathrm{proj}}{\mathrm{target}}}}{dy^{(0)}} = \frac{1}{2}(1 \pm Sy^{(0)})\frac{dN}{dy^{(0)}}\,. \tag{2}$$

In this formula, S is the slope of the R_Z dependence on rapidity that can be read out directly from the plots in the upper part of figure 2. The results of the deconvolution are shown in the plots in the lower part of figure 2. Clearly the separation between the target- and the projectile-nucleons is bigger at 1500 AMeV than it is at 400 AMeV beam energy. This means that at the higher energy the system looks more transparent. Similar results were obtained when as the "isospin-tracer" the $\frac{t}{^3\mathrm{He}}$ or the $\frac{\pi^-}{\pi^+}$ ratios were used instead of the number of protons, Z [9].

The presented method to study the mixing of the projectile- and the target-nucleons does not require any model assumptions. It is also fairly insusceptible to systematic experimental biases. Because in the end the ratios, R, for different target-projectile combinations are studied, many systematic effects cancel out. The accuracy of the results is predominantly limited by the statistical uncertainties.

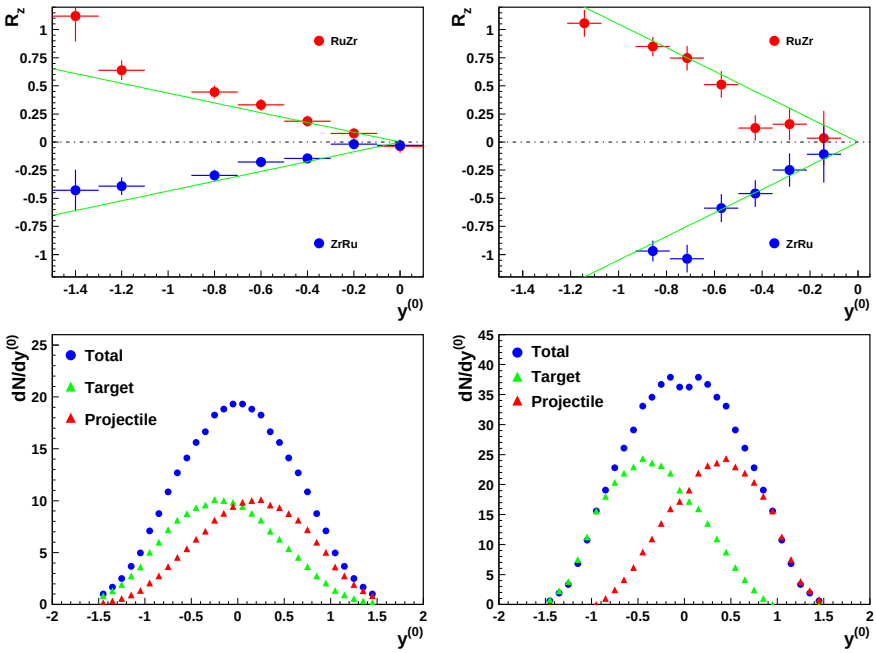

Fig. 2. Upper plots: the R_Z dependence on the scaled rapidity for central ($b <$ 2 fm) Ru+Zr and Zr+Ru collisions at 400(left) and 1500(right) AMeV beam kinetic energy. Lower plots: deconvolution of the total rapidity density distributions into separate distributions for the target- and the projectile-nucleons for reactions at 400(left) and 1500(right) AMeV beam kinetic energy.

Only recently a very systematic study on stopping based on a different approach has been completed [10]. The transverse and the longitudinal rapidity distributions of the reaction products were reconstructed for light (Ca+Ca) as well as intermediate (Ni+Ni, Ru+Ru, Xe+CsI) and heavy (Au+Au) systems at energies between 90 and 1930 AMeV. The distributions were obtained by summing up contributions from all the detected fragments, weighted with their nuclear charges. In most of the cases more than 95% of the total system charge was accounted for in this way. The distributions were also interpolated using a bi-dimensional fitting procedure in order to account for gaps in the geometrical acceptance. The variances of the resulting transverse and the longitudinal rapidity density distributions were compared. The ratio of both variances should be equal to 1 for a purely thermal spectrum. In other cases it provides a measure of the amount of stopping.

The upper-left panel in figure 3 shows the ratios of the variances (transverse to longitudinal) for 15% most central Ca+Ca and Au+Au reactions as a function of the beam energy. The upper-right panel in the figure shows the system size dependence of the variances ratios for the data taken at 400 and at 1500 AMeV beam energy. Several immediate conclusions can be drawn. The amount of stopping strongly depend on the system size, so that there is no apparent saturation even for the heaviest system studied. A pronounced maximum of stopping is observed for the heavy system between 200 and 800 AMeV beam energies; both at the lower as well as at the higher energies the amount of stopping decreases quickly. Stopping does not reach the level of purely thermal spectra, that is 1. The two last observations are obviously fully compatible with the conclusions obtained from the R_Z studies.

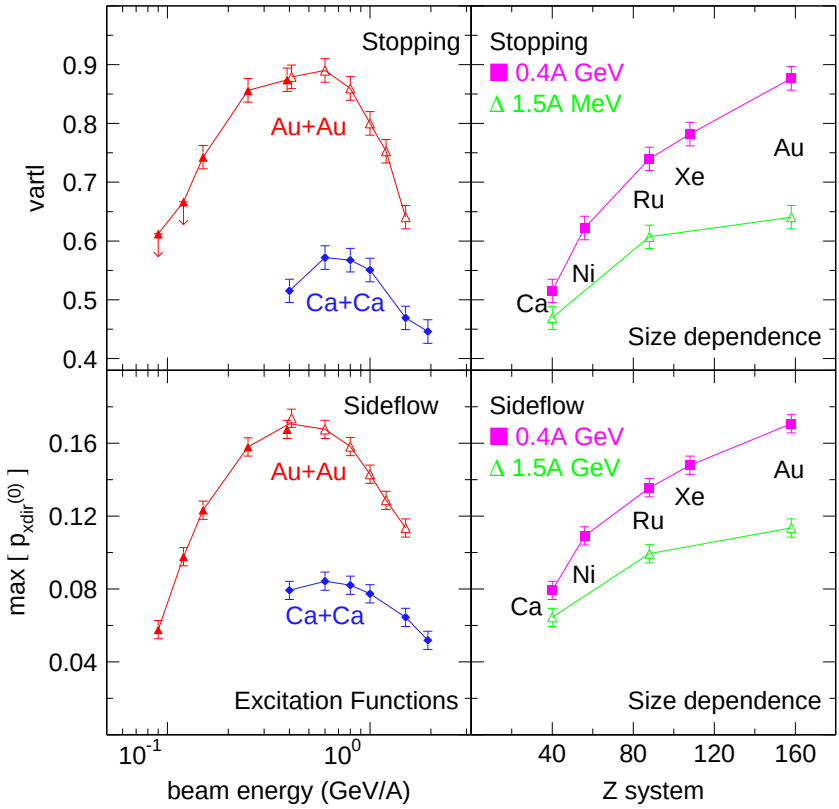

Fig. 3. Upper plots: the variances ratio (transverse to longitudinal) of the rapidity density distributions of protons; left: beam energy dependence for the Ca+Ca and Au+Au reactions; right: system size dependence at 400 and 1500 AMeV beam energy. Lower plots: similar dependencies for the maximum value of the proton sideflow in semi-central reactions.

Even more striking is the correlation of stopping with the scaled directed sideflow, defined by the following formula:

$$p_{x\mathrm{dir}}^{(0)} = \frac{\Sigma(\mathrm{sign}(y) Z u_x)}{\Sigma(Z u_{\mathrm{c.m.}}^{\mathrm{proj}})} \,. \tag{3}$$

Here, the sum runs over all the detected fragments, Z is the charge of a fragment, y and u_x are its c.o.m. rapidity and the projection of its four velocity onto the reaction plane, and $u_{\mathrm{c.m.}}^{\mathrm{proj}}$ is the projectile four velocity in the c.o.m. frame. Usually the measured amount of sideflow depends strongly on the impact parameter, and reaches a well pronounced maximum for semi-central reactions. For each system, the scaled directed sideflow of protons was studied in detail in different centrality classes, and the maximum values, $\max|p_{x\mathrm{dir}}^{(0)}|$, were determined. The lower panel in figure 3 shows the excitation function (left) as well as the system size dependence (right) of $\max|p_{x\mathrm{dir}}^{(0)}|$ for the same set of data as that presented in the upper panel. The perfect correlation of the sideflow with the amount of stopping is somehow spectacular. On the one hand, it can be quite intuitively explained. The degree of stopping presumably determines the pressure gradients in the participant matter, while this, in turn, is responsible for the amount of sideflow. On the other hand, it is clear that only a dynamical description can account for such an effect. Moreover, model calculations which aim at a realistic description of the collision dynamics are now confronted with an impressive set of data which surely provides very strong constraints on the model parameters.

As said in the Introduction, the flow of fragments is traditionally expected to depend strongly on the stiffness of the EOS. Recently, a great number of other observables are being experimentally measured and tested with model calculations to find out about their sensitivity to EOS. In order to provide stability against variation of other parameters used by the models, often ratios of similar quantities are studied. For example, the ratio of the K^+ meson multiplicities in heavy, Au+Au, to light, C+C, system, normalized to system sizes, was investigated experimentally as a function of the beam energy close to the production threshold [11]. As far as the results of the QMD model calculations are concerned, the observable was found not to depend very much on the K^+ production cross-sections, which were employed in the model, but are not known very well experimentally. The yields ratio showed however, strong sensitivity to the assumed EOS. In order to bring the results of the model calculations in agreement with the experimental findings a soft equation of state (incompressibility parameter κ=200 MeV) had to be assumed.

Quite opposite conclusions were drawn from the differential studies on the elliptic flow of fragments in semi-central Au+Au reactions at energies between 1 and 10 AGeV [12]. The second coefficients, $v_2 = \langle \cos 2\phi \rangle$, of the Fourier expansion of the azimuthal-angle distributions of protons measured at mid-rapidity ($|y_{\mathrm{c.m.}}| < 0.1$):

$$\frac{dN}{d\phi} \sim 1 + 2v_1 \cos(\phi) + 2v_2 \cos(2\phi) \tag{4}$$

were determined. Here, ϕ is the azimuthal angle of a proton with respect to the reaction plane. It was shown that the elliptic flow of protons changes the sign from negative to positive at beam energies around 4 AGeV. This effect was qualitatively reproduced by the QMD model calculations. At energies above approximately 2 AGeV the calculations with the soft EOS (κ=210 MeV) showed best agreement with the experimental data. However, in order to obtain a good agreement at lower energies a harder EOS ($\kappa = 380$ MeV) had to be introduced.

The elliptic flow of light fragments in Au+Au collisions was investigated also by the FOPI collaboration [13]. The experiments were performed in the beam-energy range which was partially overlapping with the measurements referred to above. The left panel in figure 4 shows the v_2 coefficients of the proton azimuthal-angle distributions at mid-rapidity ($|y_{\mathrm{c.m.}}| < 0.1$) obtained for semi-central Au+Au reactions at beam energies between 400 and 1500 AMeV. In the right panel in figure 4 the same variable is shown, but the analyzed distribution were obtained by summing up contributions from light fragments weighted by their masses, which in a way approximates the total amount of the elliptic flow per nucleon. In both cases the experimental data are compared to the results of the QMD model calculations with the soft as well as the hard EOS employed. As in the previous case, also here one sees that a softer EOS is needed in the model calculations in order to best reproduce the experimental data at the higher beam energies. The differences between the model results that use two distinguished EOS parametrisations are certainly bigger than the error estimate of the measurements. Nevertheless, it is important to observe that they are unfortunately not bigger than the differences between the measured proton elliptic flow and the flow of all fragments normalized to their masses. The fact that the two latter differ from each other is by itself of course not surprising. However, one has to keep in mind that currently the microscopic models do not describe very accurately the measured mass distributions of the produced fragments. About 30% of the detected protons are bound in fragments at 1500 AMeV beam energy. This number grows to about 65% as the beam energy decreases to 400 AMeV. The amount of clusters predicted by models is much less than this. Therefore, in the current situation, comparison of the model results on

the elliptic flow of protons or fragments to the corresponding experimental data is questionable in general. In particular, the conclusions about the EOS drawn from such comparison, which in earlier days was believed to have a strong phenomenological basis, cannot be easily justified.

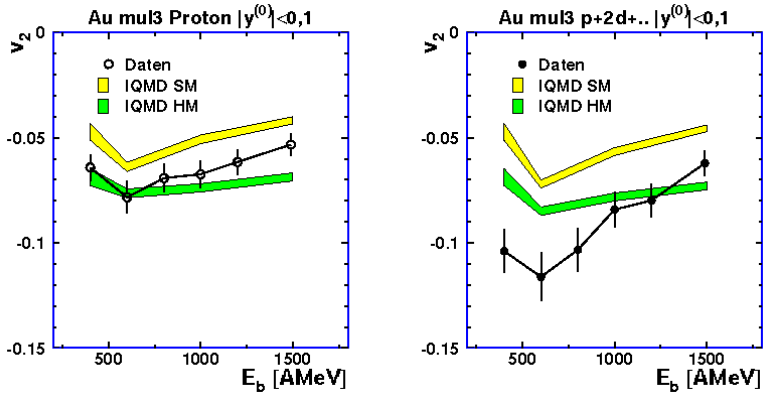

Fig. 4. Left: the v_2 coefficients of the proton azimuthal-angle distributions at mid-rapidity ($|y_{\mathrm{c.m.}}| < 0.1$) obtained for semi-central Au+Au reactions at beam energies between 400 and 1500 AMeV. Right: the same variable but the studied azimuthal-angle distributions were obtained by summing up contributions from light fragments weighted by their masses.

4. Production of strange baryons and mesons

Traditionally, strange particles are considered to probe the early phase of heavy-ion collisions. There is a lot of experimental data on the production of charged kaons at intermediate beam energies [14]. Less is known about neutral particles, such as $K^0$and Λ. In particular, phase-space distributions of these reactions products are usually not measured with a good accuracy.

In the FOPI detector, neutral strange particles are identified by the reconstruction of the invariant mass of their decay products ($K^0 \to \pi^+\pi^-$, $\Lambda \to \pi^- p$). Due to the detector dimensions, only K^0_{S} can be reconstructed from all the K^0mesons produced in the reactions. On the other hand, the reconstructed Λ hyperons include also those coming from the $\Sigma^0 \to \Lambda\gamma$ decay. In other words, in the FOPI detector Λ and Σ^0 hyperons are not distinguishable.

Figure 5 shows the K^0_{S} and Λ transverse-mass spectra ($m_{\mathrm{t}}{=}\sqrt{p_{\mathrm{t}}^2{+}m_0^2}$) measured in different rapidity bins (indicated in the figure), in central (350 mb) Ni+Ni collisions at 1930 AMeV beam energy [15]. The spectra are corrected for the detection efficiency estimated by means of the GEANT simulation of a complete detector response, which includes the front-end electronics signal

processing and shaping. The spectra are multiplied by subsequent factors of 10 in order to allow presentation in one figure. As can be seen from the figure, no extrapolation due to the detector geometrical acceptance at low m_t is needed. It is also demonstrated that the yields, both of $K^0$and of Λ drop exponentially with rising m_t . The fits of the corresponding exponential curves are indicated in the figure.

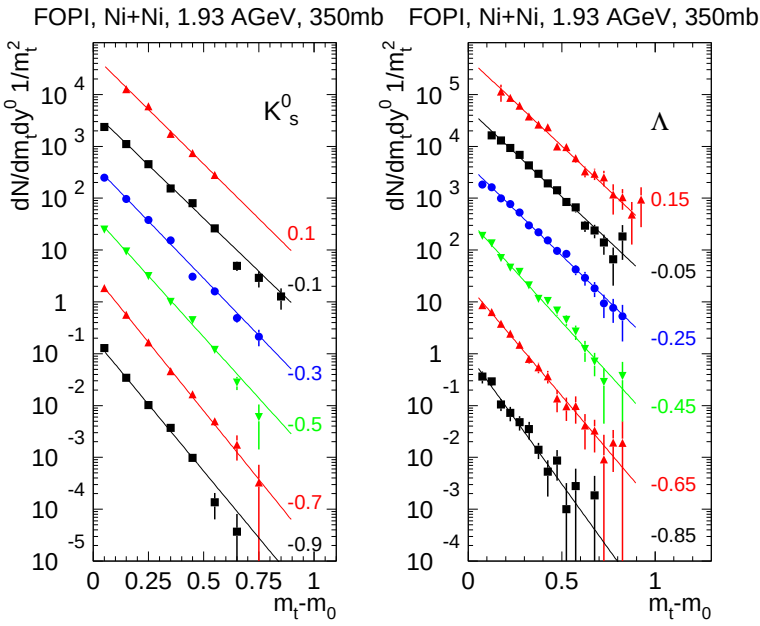

Fig. 5. K^0_S and Λ transverse-mass spectra measured in central (350 mb) Ni+Ni collisions at 1930 AMeV beam energy.

Figure 6 shows the corresponding rapidity density distributions derived from the m_t -spectra by integrating the yields under the fitted curves. The distributions were corrected for the branching ratios into the respective decay channels (68.6% for K^0_S and 63.9% for Λ). In addition, the original yields of K^0_S were multiplied by a factor of two in order to take into account also K^0_L mesons. The resulting rapidity density distribution of K^0mesons is compared to those of K^+ mesons measured by the FOPI and by the KaoS collaborations [16]. It can be seen that the yields and the widths of the phases-space distributions of the charged and the neutral kaons are very similar.

The rapidity density distribution of Λ hyperons is shown in the right panel in figure 6. Agreement between two independent sets of data is demonstrated. The distribution is compared to the rapidity density distribution of protons scalded by a factor of 260. The phase-space distribution

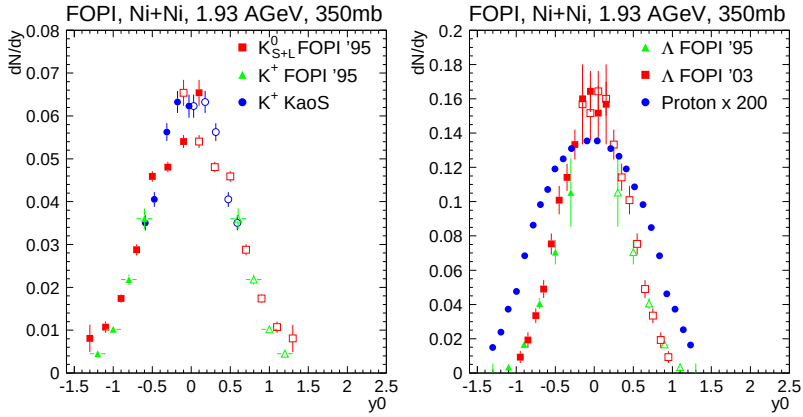

Fig. 6. $K^0$and Λ rapidity density distributions measured in central (350 mb) Ni+Ni collisions at 1930 AMeV beam energy.

of Λ hyperons is more compact than that of protons. This observation suggests again that global equilibrium among baryons is not reached during the reactions. The width of the Λ distribution, 0.42±0.02, can be also compared to the width predicted by the IQMD model with momentum dependent Λ–N interactions: 0.38, and to the width resulting from UrQMD simulations: 0.44 [17].

Both the Λ hyperon as well as the K^0meson rapidity density distributions shown in figure 6 are measured in the backward hemisphere. Because, in this case, symmetric reactions were studied, the data can be reflected with respect to the mid-rapidity, so that no further extrapolation to the full solid angle is necessary. The integrated yields per collision extracted for all the measured strange particles are listed in Table I. In addition, an estimate for the K^- meson yield is given [18]. Since anti-strange mesons (K^0, K^+) are co-produced either with strange baryons (Λ, $\Sigma^{0,\pm}$) or with strange mesons (K^-), the sum of the K^+ and K^0meson yields should be equal to that of the Λ and $\Sigma^{0,\pm}$ hyperons plus a small contribution from the K^- mesons. Comparison of the numbers given in Table I leads to the conclusion that the combined yield of Λ and Σ^0 hyperons exhausts to a large extent the yield allowed for strange hyperons that could be produced together with anti-strange K^+ and K^0mesons. Because of the strangeness conservation, the balance between the strange and the anti-strange quarks cannot be changed during the reactions. This would mean that either only a relatively small number of $\Sigma^\pm$ hyperons are produced, or that the produced charged hyperons are likely to be re-absorbed and converted into the neutral ones in the surrounding participant matter. If the preliminary numbers presented in Table I do not change, this observation will have to be understood in more detail.

TABLE I

Strange and anti-strange meson and baryon yields per central (350 mb) Ni+Ni collision at 1930 AMeV beam kinetic energy.

	K^+	K^0	Λ+Σ^0	K^-
yield per collision	0.085(10)	0.085(10)	0.15(1)	0.003(1)

In the recent Ni+Ni experiment at 1930 AMeV beam kinetic energy more than 120 million central and semi-central (750 mb) events were recorded, and altogether more than 120 thousand Λ hyperons were reconstructed. With such a large statistics, correlations of Λ with other reaction products can be studied. Recently the existence of very dense clusters consisting of several nucleons and a K^- meson was postulated [19]. For example, a bound state of $ppnK^-$ system was predicted to have the binding energy of 108 MeV, the width of $\Gamma = 20$ MeV, and is expected to decay into $\Lambda\, d$ pair. Preliminary analysis of the Ni+Ni data indicates indeed an excess in the invariant mass of the reconstructed $\Lambda\, d$ pairs at about 3.2 GeV. This very interesting result is certainly worth further investigation.

5. Summary and conclusions

In this contribution we reported on the recent results obtained by the FOPI collaboration from heavy-ion experiments performed at beam energies in the range between 90 and 1930 AMeV. We addressed the question of the reaction dynamics in several different ways. By means of the isospin-tracer method, we showed that the total measured rapidity density distributions can be deconvoluted into separate distributions of the target- and the projectile-nucleons which do not fully mix. We showed that the transverse rapidity distributions are narrower than the longitudinal ones and that the ratio of the variances of these distributions is smaller than expected from the fully stopped scenario. We demonstrated that the amount of stopping measured by the variances ratio is strongly correlated to amount of sidefow. We presented a rather complete systematics on both the stopping as well as the flow, which certainly provides a lot of information to be confronted with results of model calculations. We pointed out that more understanding of the fragment formation in transport models is needed before conclusions from the comparison to the experimental data can be justified. We also reported on the reconstruction of the neutral strange particles. We showed the phase-space distributions of $K^0$and Λ measured down to low transverse momenta and in the complete rapidity range, from the target- to the mid-rapidity. By

comparing the rapidity density widths, we argued that the equilibrium is not reached between strange and non-strange baryons in the course of the reactions. We studied the balance between the strange and the anti-strange quarks contained in all the measured reaction products. We found out that quite small number of $\Sigma^{\pm}$ hyperons is allowed in the final state in order not to violate the strangeness conservation rule. Finally, we pointed out to a very exciting, possibly completely new physics of highly dense clusters made of nucleons and K^- mesons, for which the evidence may be found in the existing data.

REFERENCES

[1] R. Stöcker, W. Greiner, *Phys. Rep.* **137**, 277 (1986).
[2] D.B. Kaplan, A.E. Nelson, *Phys. Lett.* **B175**, 57 (1986).
[3] C. Fuchs, T. Gaitanos, *Nucl. Phys.* **A714**, 643 (2003).
[4] J. Cleymans *et al., Phys. Rev.* **C57**, 3319 (1998).
[5] P. Danielewicz, R. Lecay, W.G. Lynch, *Science* **298**, 1592 (2002).
[6] E.L. Bratkovskaya, W. Cassing, *Nucl. Phys.* **A619**, 413 (1997).
[7] J. Ritman *et al., Nucl. Phys.* **B44**, 708 (1995).
[8] F. Rami *et al., Phys. Rev. Lett.* **84**, 1120 (2000).
[9] Y.J. Kim *et al.,* in preparation.
[10] W. Reisdorf *et al.,* submitted to *Phys. Rev. Lett.*
[11] C. Sturm *et al., Phys. Rev. Lett.* **86**, 39 (2001).
[12] C. Pinkenburg *et al., Phys. Rev. Lett.* **83**, 1295 (1999).
[13] T. Kress, PhD thesis, TU Darmstadt, 2002; A. Andronic *et al.,* in preparation.
[14] A. Foerster *et al., Phys. Rev. Lett.* **91**, 152301 (2003); K. Wisniewski *et al., Eur. Phys. J.* **A9**, 515 (2000).
[15] K. Wisniewski *et al.,* in preparation.
[16] D. Best *et al., Nucl. Phys.* **A625**, 307 (1997); P. Senger, private communication.
[17] Y. Leifels, private communication.
[18] A. Mangiarotti *et al.,*, *Nucl. Phys.* **A714**, 89 (2003).
[19] Y. Akaishi, T. Yamazaki, *Phys. Rev.* **C65**, 044005 (2002).